Chemical Science

ROYAL SOCIETY OF CHEMISTRY

EDGE ARTICLE

View Article Online
View Journal | View Issue

Cite this: *Chem. Sci.*, 2025, **16**, 21498

All publication charges for this article have been paid for by the Royal Society of Chemistry

Received 30th July 2025
Accepted 7th October 2025

DOI: 10.1039/d5sc05740j

rsc.li/chemical-science

Ligand-controlled divergent enantioselective hydroarylation of cyclobutenes

Renming Pan,†[a] Jie Zhu,†[b] Xinjie Zhou,†[a] Minyan Wang*[b] and Ping Lu *[ac]

The palladium-catalyzed enantioselective redox-neutral coupling of alkenes with organoboronic reagents remains an unfulfilled challenge. Herein, we report a divergent palladium-catalyzed enantioselective hydroarylation of cyclobutenes with arylboronic acids, affording both 1,2- and 1,3-hydroarylation products. The regioselectivity was tuned by judicious choice of chiral ligands. The palladium-hydride species was generated from a palladium catalyst and arylboronic acid or *in situ* generated HOAc, as supported by deuterated experiments and density functional theory (DFT) calculations. We anticipate that this redox-neutral coupling with organoboronic reagents could stimulate interest in other unsaturated alkene systems.

Introduction

The palladium-catalyzed functionalization of alkenes represents one of the powerful strategies for constructing carbon–carbon bonds.[1–6] Owing to their convenient manipulation and low toxicity, the cross-coupling reaction of organoboron reagents with alkenes has attracted tremendous attention.[7] Among them, significant progress has been made in the enantioselective oxidative coupling of alkenes, which includes the oxidative Heck reaction and the redox-relay Heck process.[3,8–15] An oxidant is usually required to re-oxidize Pd(0) to Pd(II) to complete the catalytic cycle. Thus, the use of chiral phosphorus ligands in these reactions is limited.

On the other hand, the palladium-catalyzed reductive coupling of alkenes with organoboron compounds has been less explored. While the palladium-catalyzed enantioselective conjugate addition of arylboronic acids to acceptor-substituted alkenes is known,[16–18] the hydroarylation of electronically non-biased alkenes is still a formidable challenge. Sigman reported an elegant palladium-catalyzed reductive coupling of styrenes and 1,3-dienes with arylboronic esters, utilizing *in situ* generated palladium hydride species from isopropanol under an aerobic atmosphere.[19–21] However, only moderate enantioselectivity has been achieved for the asymmetric hydroarylation of styrene (Scheme 1a).[21] Engle disclosed a directing group-assisted regioselective hydroarylation of unactivated alkenes *via* an arylpalladium intermediate in a non-enantioselective manner.[22] In these approaches, a stabilized palladium intermediate was formed, allowing it to outcompete β-hydride elimination effectively. In comparison, the nickel-catalyzed hydroarylation of alkenes with arylboronic acids has emerged as an efficient redox-neutral approach.[23–32] Although Ni-catalyzed asymmetric hydroarylations have been reported, the alkenes are primarily limited to styrenes and 1,3-dienes.[25–27] Hence, the development of a catalyst system remains in demand to achieve the enantioselective redox-neutral coupling of various alkenes with organoboronic reagents.

Cyclobutenes, as a class of strained alkenes, exhibit characteristic reactivity and unique properties in synthetic and medicinal chemistry.[33,34] A variety of enantioenriched cyclobutane derivatives have been prepared by the precise functionalization of four-membered carbocycles with versatile catalytic systems.[35–44] One challenge of this strategy is the undesired ring-opening reaction, driven by the release of strain energy. For instance, it has been reported that a palladium-catalyzed coupling of the parent cyclobutene with arylboronic acids resulted in ring-opening products under aerobic conditions, instead of the hydroarylation product (Scheme 1b).[45] Therefore, the catalytic system is essential for the success of the desired hydroarylation. In addition, versatile multi-substituted cyclobutanes with diverse chemical space could be obtained from divergent hydroarylation of cyclobutenes. Initiated by enantioselective carbometallation, diversified functionalization of cyclobutenes was developed by Fletcher[46] and us[47] (Scheme 1c). These diverse reaction pathways were tuned by coupling reagents and cyclobutene substrates. We wondered whether divergent asymmetric functionalization of cyclobutenes with arylboronic acids could be achieved through the control of the catalytic system.

[a]*Research Center for Molecular Recognition and Synthesis, Department of Chemistry, Fudan University, 220 Handan Lu, Shanghai 200433, P. R. China. E-mail: plu@fudan.edu.cn*

[b]*State Key Laboratory of Coordination Chemistry, Chemistry and Biomedicine Innovation Center (ChemBIC), School of Chemistry and Chemical Engineering, Nanjing University, Nanjing 210093, P. R. China. E-mail: wangmy@nju.edu.cn*

[c]*State Key Laboratory of Green Chemical Synthesis and Conversion, Fudan University, Shanghai, P. R. China*

† These authors contributed equally.

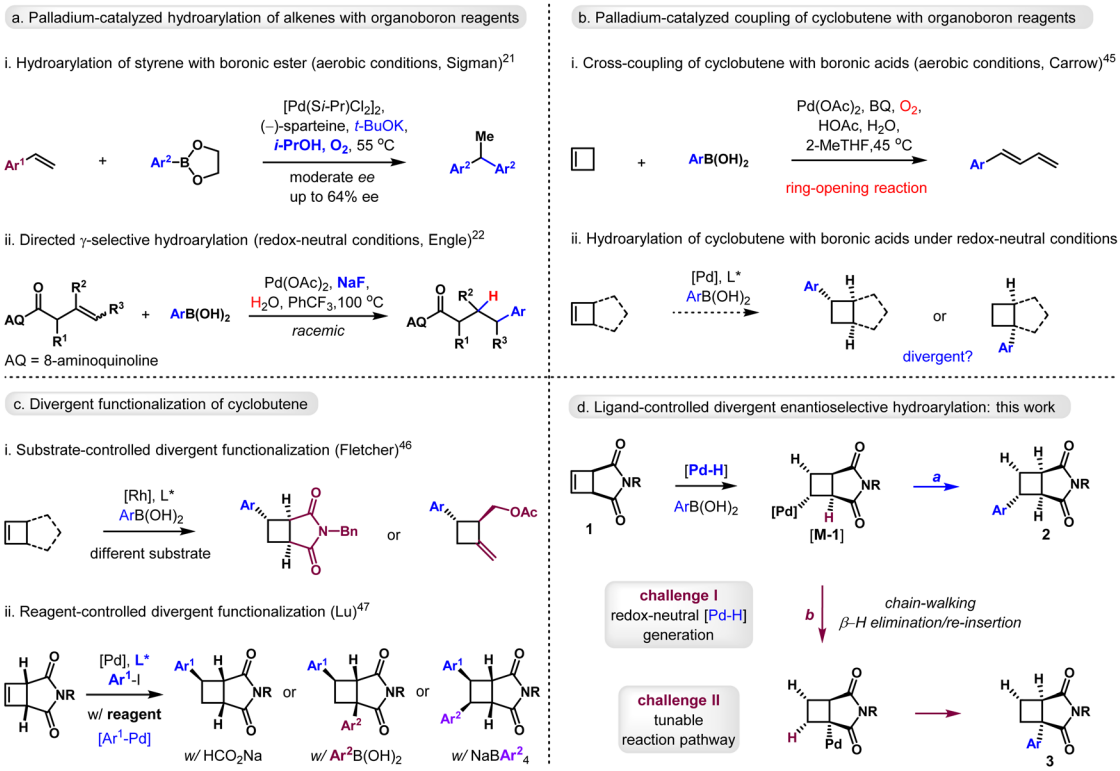

Scheme 1 Palladium-catalyzed hydroarylation of alkenes with organoboron reagents.

It is well known that the oxidative addition of Pd(0) with a weak acid affords palladium hydride species, which enables versatile hydrofunctionalization.[48–61] It was reported that ammonium salt (NEt_3H^+, pK_a in H_2O, 10.75) could be used as an acid source for Pd–H formation.[62] We speculated that the Pd–H species may be *in situ* generated from Pd(0) and phenylboronic acid (pK_a in H_2O, 8.72)[63] without an external acid. Initiated by Pd–H species, two reaction pathways could occur from intermediate **M-1**, leading to the formation of 1,2- or 1,3-hydroarylation products, respectively (Scheme 1d). To achieve these, two challenges have to be addressed: (1) the generation of Pd–H species under redox-neutral conditions and (2) the control of the two possible reaction processes.

Herein, we report our work on the palladium-catalyzed divergent enantioselective reductive coupling of cyclobutenes and arylboronic acids to provide 1,2- and 1,3-hydroarylation products. The Pd–H species was generated from the palladium catalyst with arylboronic acid or *in situ* generated HOAc, and the reaction pathways were controlled by the chiral ligands. Preliminary mechanistic insights and the origin of enantioselectivity were explained by deuterium labeling experiments and density functional theory (DFT) calculations.

Results and discussion

We commenced our studies with the reaction of cyclobutene **1a** and phenylboronic acid using a palladium catalyst and chiral phosphorus ligands (Scheme 2). The reaction furnished both racemic 1,2-hydroarylation product **2a** and the migratory 1,3-hydroarylation product **3a**, with a combined yield of 26% and a ratio of 1.2 : 1 when (*R*)-BINAP (**L-1**) was employed. Further screening of chiral ligands revealed that *P*-stereogenic ligand **L-3** provided both **2a** and **3a** with moderate enantioselectivity. The optimal results for the 1,3-hydroarylation were identified using (*S*)-BI-DIME (**L-4**), which afforded product **3a** in 88% yield and 93% ee. It is noteworthy that the enantioselectivity for the minor regioisomer **2a** was only 23% ee.

Interestingly, the hydroarylation selectivity switched when the catalytic system was exposed to water. In the presence of five equivalents of water, 1,2-hydroarylation product **2a** became the major product, although the enantioselectivity was only 25%. Excellent regioselectivity was observed when using $Pd(dmdba)_2$ as the catalyst, which provided cyclobutane **2a** exclusively in good yield. With $Pd(dmdba)_2$ as the catalyst and water as an additive, ligand screening revealed that (*S*,*S*)-Ph-BPE (**L-7**) was an effective ligand, leading to product **2a** in 81% yield and 70% ee. Further optimization of reaction parameters revealed that the reactivity was greatly influenced by the amount of water. With $Pd(OAc)_2$ and **L-7**, the reaction gave a low conversion in the presence of H_2O (9%, 66% ee). In contrast, high yield and good enantioselectivity were achieved when 5 Å molecular sieves were used as additives (86%, 83% ee). Optimal results were obtained using DME as solvent, and the reaction provided 1,2-hydroarylation product **2a** in 68% yield and 92% ee.

With optimal conditions identified, the substrate scope of enantioselective 1,2-hydroarylation was examined (Table 1). Initially, a group of *para*-substituted phenylboronic acids were evaluated. Various electron-rich substituents were tolerated,

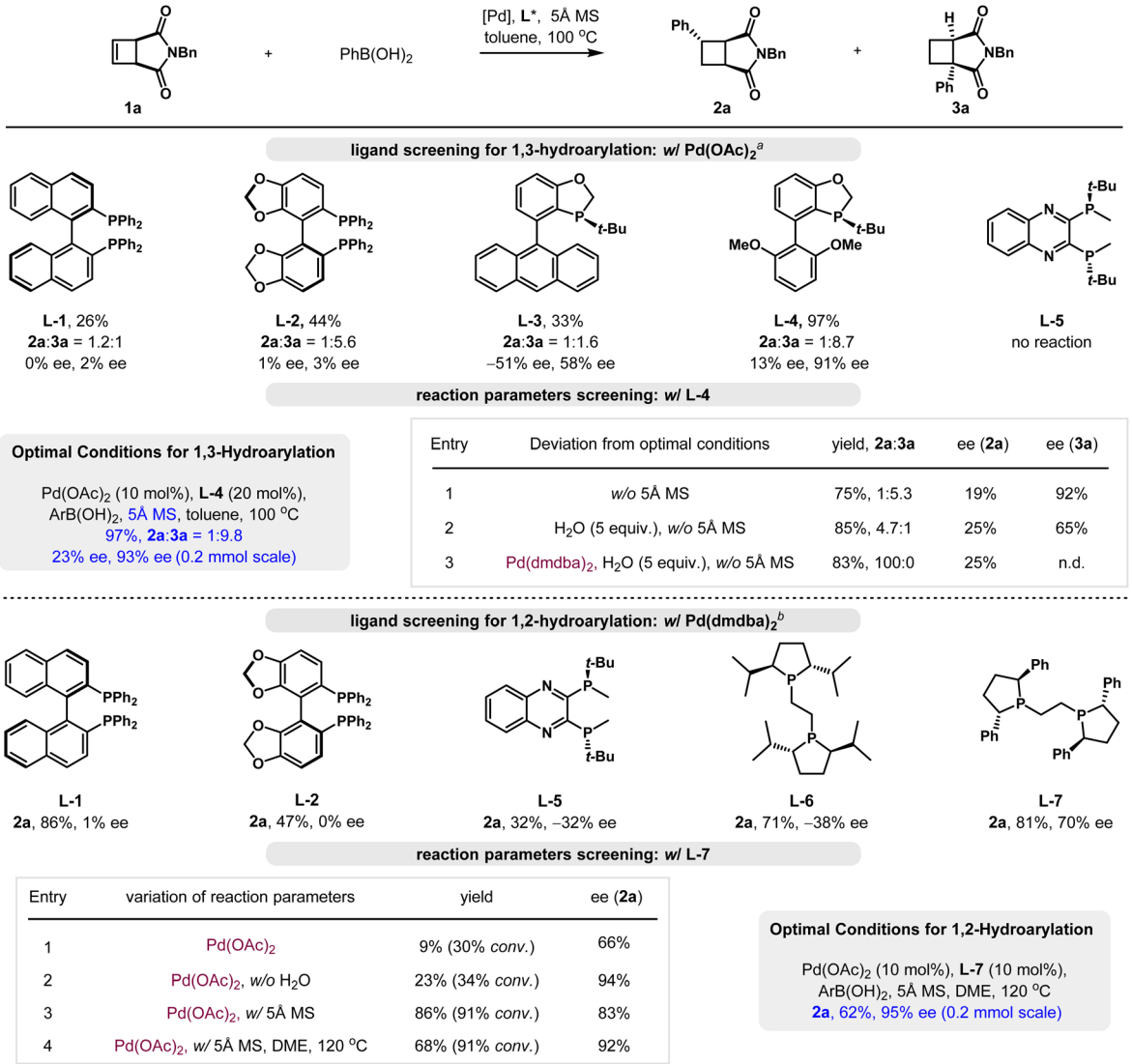

Scheme 2 Reaction optimization. Reaction conditions: [a]**1a** (0.1 mmol), $PhB(OH)_2$ (2–3 equiv), [Pd] (10 mol%), L* (10–20 mol%), 5 Å MS, toluene, 100 °C, 7–48 h. [b]H_2O (5 equiv.) was used as an additive, without 5 Å MS; in the case of 5 Å MS, no H_2O was added. dmdba = 3,5,3′,5′-dimethoxydibenzylideneacetone. See the SI for optimization details.

including methyl (**2b**), methoxy (**2c**), *tert*-butyl (**2d**), trimethylsilyl (**2e**), and phenyl (**2f**) groups, giving the corresponding products in 92–97% ee. Notably, enantioselectivity varied with different palladium catalysts, with $Pd_2(dba)_3 \cdot CHCl_3$ leading to better results in some cases. A variety of electron-withdrawing groups were also examined, and substituents such as chloro (**2g**), trifluoromethyl (**2h**), formyl (**2i**), acetyl (**2j**), methoxycarbonyl (**2k**), and nitrile (**2l**) groups were effectively introduced. The enantioselectivities were in the range of 83–94%. Both *meta*- and *ortho*-substituted phenylboronic acids were applicable, giving the corresponding products **2m–2o** in 81–88% ee. 2-Naphthyl and disubstituted phenyl boronic acids were compatible as well, affording cyclobutanes **2p–2r** in 82–93% ee. Additionally, the heteroaryl substituents were efficiently installed, including thiophen-3-yl (**2s**, 80% ee) and dibenzo[*b*,*d*]thiophen-2-yl (**2t**, 92% ee) groups. In contrast to our previous palladium-catalyzed cross-coupling of cyclobutenes with aryl halides,[47] substrates 3-azabicyclo[3.2.0]hept-6-ene-2,4-diones **1b** and **1c** were applicable, furnishing the cyclobutanes **2u** and **2v** in 92–96% ee.

The substrate scope of enantioselective 1,3-hydroarylation of cyclobutene is summarized in Table 2. An array of *para*-substituted phenylboronic acids were compatible under optimal conditions, and substituents including methyl (**3b**), *tert*-butyl (**3d**), trimethylsilyl (**3e**), phenyl (**3f**), chloro (**3g**), trifluoromethyl (**3h**), formyl (**3i**), acetyl (**3j**), methoxycarbonyl (**3k**), and nitrile (**3l**) were installed in good enantioselectivities, except for methoxy (**3c**), which was isolated in 76% ee. Additionally, a group of *meta*-substituted phenylboronic acids were tolerated, affording the corresponding products **3m–3o** with enantioselectivities ranging from 87% to 95% ee. 2-Naphthyl and disubstituted phenyl groups could be introduced at the

Table 1 Substrate scope of 1,2-hydroarylation[a]

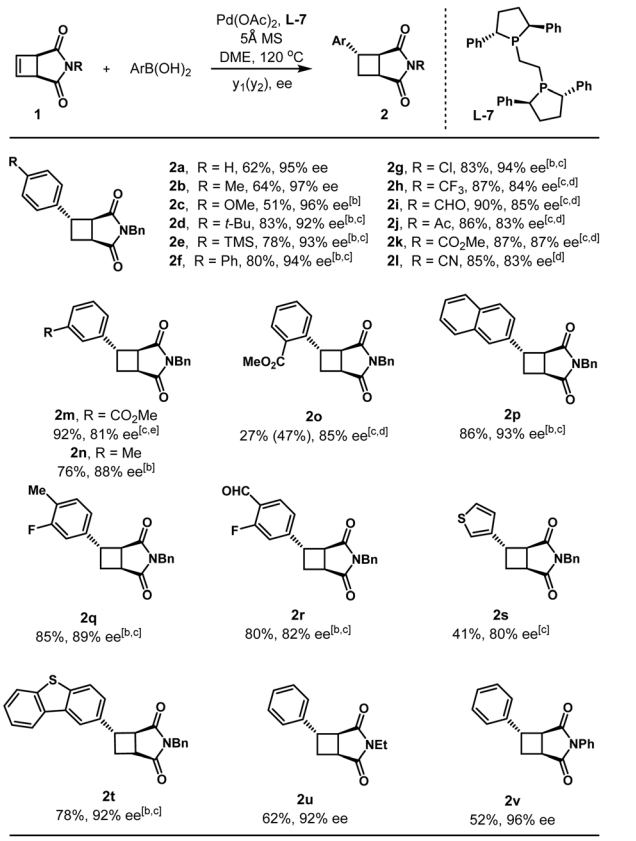

[a] **1** (0.2 mmol), $ArB(OH)_2$ (3.0 equiv) $Pd(OAc)_2$ (10 mol%), **L-7** (10 mol%), DME, 5 Å MS, 120 °C, 48–72 h; yield in parenthesis is based on the recovered starting material. [b] 100 °C. [c] $Pd_2(dba)_3 \cdot CHCl_3$ (5 mol%) was used. [d] 80 °C. [e] 60 °C.

Table 2 Substrate scope of migratory 1,3-hydroarylation[a]

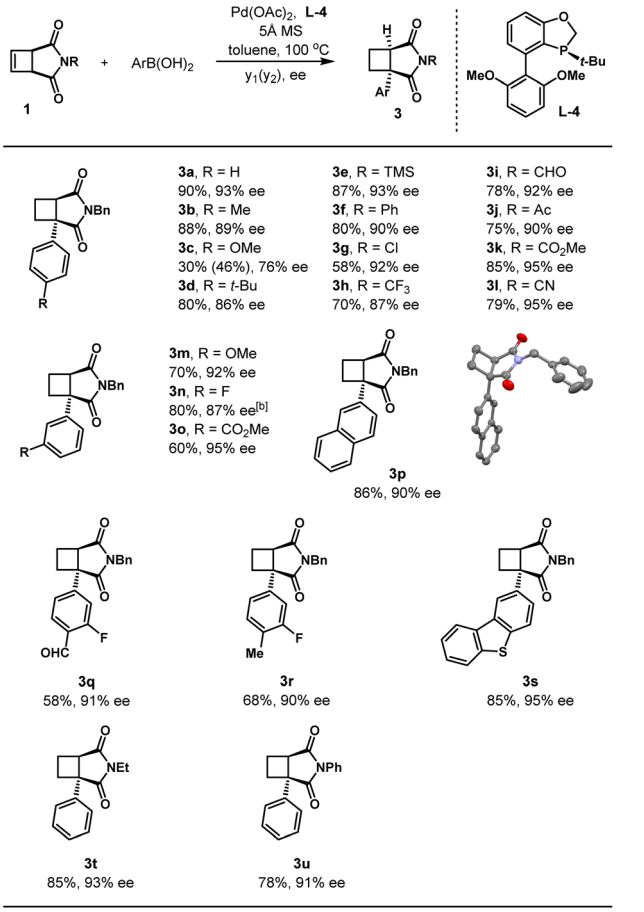

[a] **1** (0.2 mmol), $ArB(OH)_2$ (2.0 equiv), $Pd(OAc)_2$ (10 mol%), **L-4** (20 mol%), toluene, 5 Å MS, 100 °C, 10–24 h; yield in parenthesis is based on the recovered starting material. [b] 80 °C.

angular position smoothly, furnishing azabicyclic products **3p**–**3r** in 58–86% yield and 90–91% ee. In addition, dibenzo[*b*,*d*] thiophen-2-ylboronic acid was also tolerated, giving the heteroaryl substituted product **3s** in 85% yield and 95% ee. Furthermore, the reaction of cyclobutenes **1b** and **1c** provided the corresponding 1,3-hydroarylation products **3t** and **3u** smoothly in 91–93% ee. The absolute structure of **3p** was unambiguously determined by the single-crystal X-ray analysis.

To shed light on the reaction mechanism, we first conducted deuterium labeling experiments for 1,2-hydroarylation. The reaction of deuterated cyclobutene **1a-D** with phenylboronic acid provided product **2a-D-a** in 70% yield and 92% ee under standard 1,2-hydroarylation conditions (Scheme 3a). The recovered **1a-D** was isolated in 8% yield, with deuterated atoms remaining intact. When deuterated phenylboronic acid (contaminated with 18 mol% $(PhBO)_3$) was employed, the reaction of **1a** afforded product **2a-D-b** in 85% yield and 82% ee, with 51% deuterium incorporation at the C(7) position (Scheme 3b). Without 5 Å MS, **2a-D-b** was obtained with a higher deuterium (0.70D) incorporation (Scheme 3c). These findings suggested that a hydrogen/deuterium (H/D) exchange existed, and protons in 5 Å MS[64,65] resulted in a lower deuterium incorporation. Interestingly, a H/D exchange was also observed when cyclobutene **1a-D** was exposed to the standard conditions in the absence of phenylboronic acid (Scheme 3d). We hypothesized that a concerted metalation-deprotonation (CMD) pathway may occur, leading to the loss of deuterium incorporation.[66–70]

The deuterium labeling experiments for migratory 1,3-hydroarylation were then performed. The reaction of cyclobutene **1a** with deuterated phenylboronic acid afforded migratory product **3a-D-a** in 74% yield and 91% ee, with deuterium atoms incorporated at the C (5–7) positions (Scheme 3e). Meanwhile, 1,2-hydroarylation product **2a-D-c** was isolated in 20% yield and 25% ee, with deuterium atoms incorporated at the C (1, 5, and 7) positions. Deuterium atoms were introduced at the angular position for both products. In the absence of 5 Å MS, the reaction furnished hydroarylation product **3a-D-a** in 56% yield and 82% ee with slightly higher distribution of deuterium. In comparison, the reaction of **1a-D** with

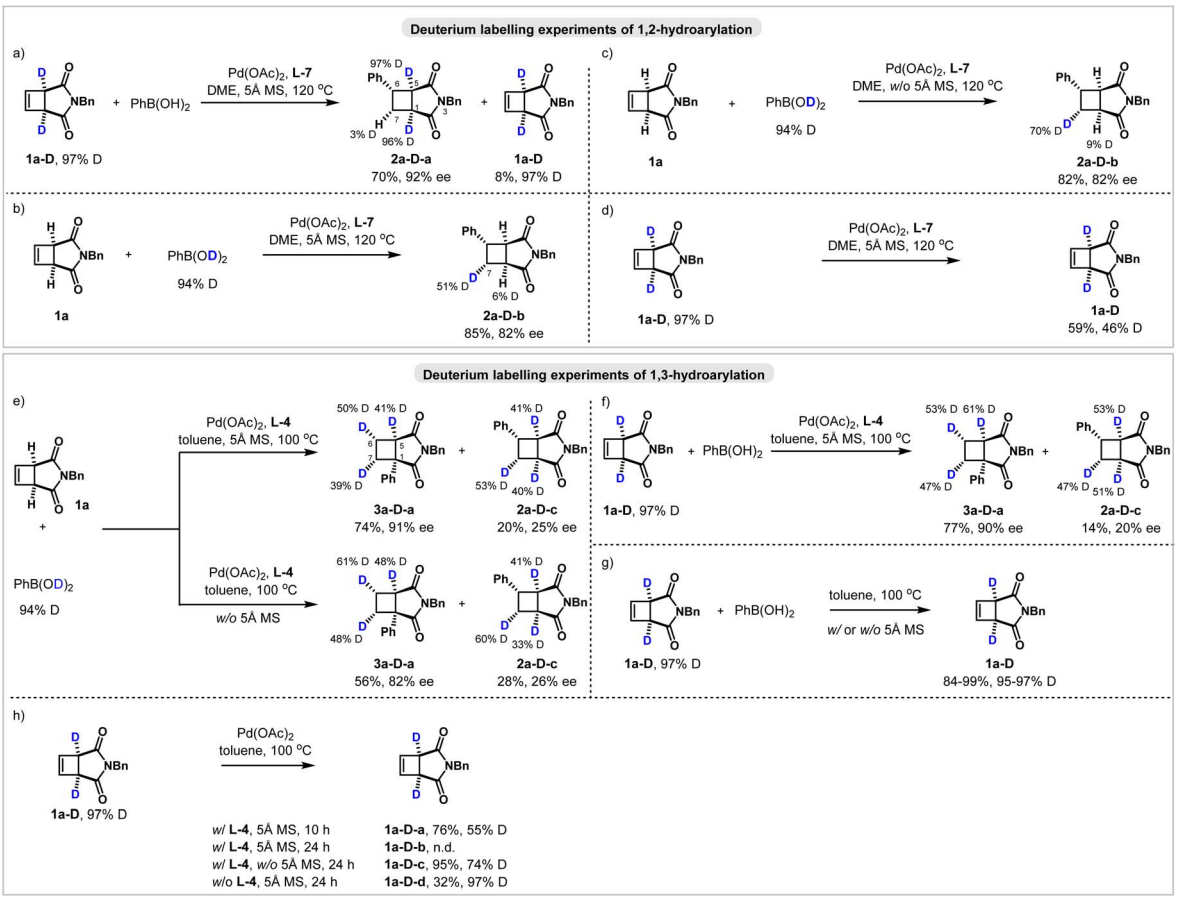

Scheme 3 Deuterium labelling experiments of hydroarylation.

phenylboronic acid provided both product **3a-D-a** and product **2a-D-c**, showing a similar distribution of deuterium (Scheme 3f).

The possibility of H/D exchange between **1a-D** and $PhB(OH)_2$ was examined. In the absence of a palladium catalyst, no H/D exchange was observed, regardless of the presence of 5 Å MS (Scheme 3g). The roles of **L-4** and 5 Å MS were also investigated in the absence of $PhB(OH)_2$. When using Pd/**L-4**, a facile H/D exchange was observed, suggesting that a CMD pathway likely took place (Scheme 3h). Of note, complete decomposition of **1a-D** occurred after 24 h. Without 5 Å MS, cyclobutene **1a-D** remained intact, with a lesser extent of deuterium loss (74% D) after 24 h. Furthermore, deuterium atoms in **1a-D** remained unaffected without **L-4**, while partial decomposition was observed in the presence of 5 Å MS.

To gain a comprehensive understanding of the underlying reaction mechanism and the origin of enantioselectivity, extensive density functional theory (DFT) calculations were performed on a model reaction between cyclobutene **1a** and phenylboronic acid in different ligand environments.[71] The calculated energy profile for the formation of product **2a** in the presence of ligand **L-7** is shown in Scheme 4a, where the *in situ* generated Pd(0) species **INT1A-L7** is designated as the reference zero point for Gibbs free energy. Initially, the oxidative addition of the O–H bond in $PhB(OH)_2$ to the Pd(0) center occurs *via* the transition state **TS2A-L7**, which necessitates surmounting an activation energy barrier of 13.2 kcal mol^{-1}. An exploration into the feasibility of the oxidative addition of the O–B bond in $PhB(OH)_2$ reveals that this pathway is reversible and only needs to overcome an energy barrier of 1.6 kcal mol^{-1}. As a consequence of these reaction characteristics, both Pd(II)–H and Pd(II)–Ph species are present simultaneously in the reaction system. The migratory insertion of cyclobutene into the Pd(II)–H species **INT2A-L7** represents the enantio-determining step. The energy barrier of the pathway leading to the experimentally observed 1*S*,5*R*,6*S*-configuration *via* transition state **TS3A-L7-5R6S** is 13.1 kcal mol^{-1} relative to **INT2A-L7**, which is more energetically favorable than other pathways passing through transition states **TS3A-L7-5S6R**, **TS3A-L7-5R6R**, and **TS3A-L7-5S6S** (13.1 *vs.* 14.4, 16.9, and 15.5 kcal mol^{-1}).

The origin of enantioselectivity can be further elucidated through the stereochemical models (Scheme 4b).

In the transition states **TS3A-L7-5R6S** and **TS3A-L7-5S6R**, C–H···π interactions (2.33 and 2.45 Å respectively) exist between the C–H bond of cyclobutenes and the phenyl group in the **L-7** ligand. When comparing with **TS3A-L7-5S6R**, the relatively stronger C–H···π interactions in **TS3A-L7-5R6S** significantly stabilize the transition state structure, lower the activation

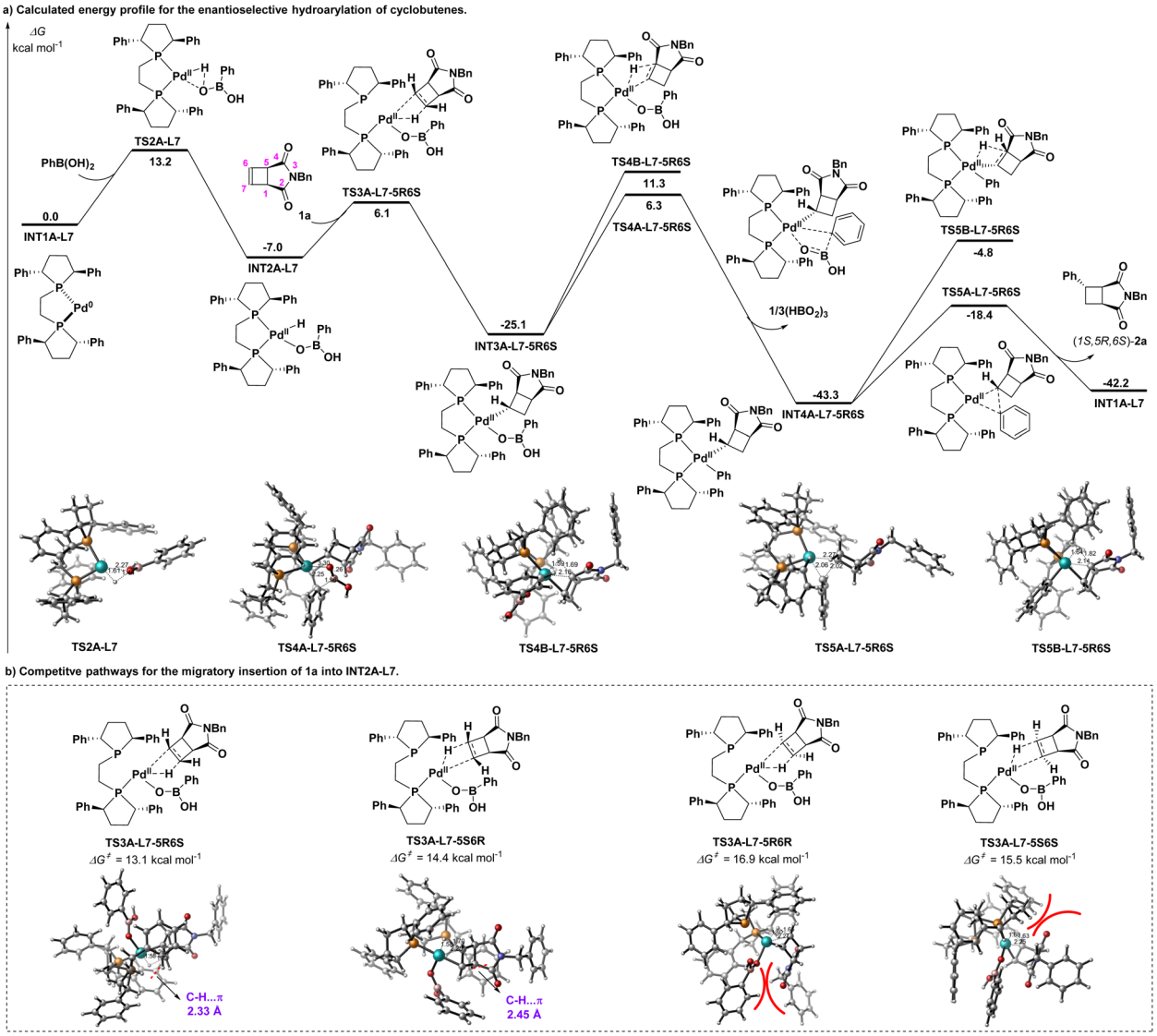

Scheme 4 DFT investigations for the enantioselective 1,2-hydroarylation of cyclobutenes in the presence of L-7.

energy barrier, and facilitate the formation of the chiral intermediate **INT3A-L7-5R6S**. In contrast, within the unfavorable transition states **TS3A-L7-5R6R** and **TS3A-L7-5S6S**, the spatial configuration in which the substituents of cyclobutene and the chiral ligand are oriented in the same direction results in a significant surge in steric repulsion, directly resulting in the elevation of the energy barriers of these two transition states. Taking into account the significantly high energy barriers calculated for the migratory insertion pathway of cyclobutene with the Pd(II)–Ph species, this reaction mechanism was ultimately deemed unfeasible and excluded (Fig. S13). The calculation results indicate that deuterium atoms can be transferred from phenylboronic acid to the C7 position of the product (1*S*,5*R*,6*S*)-**2a**, which is consistent with the observations from the deuterium-labeling experiments (Scheme 3b and c). Subsequently, the favorable intermediate **INT3A-L7-5R6S** undergoes β-carbon elimination[72–74] *via* the transition state **TS4A-L7-5R6S** with an energy barrier of 31.4 kcal mol^{-1} to form the intermediate **INT4A-L7-5R6S**. This step, which corresponds to the highest energy barrier in the energy profile, is designated as the rate-determining step in the catalytic cycle. This designation is in good agreement with the kinetic experiments of 1,2-hydroarylation. In these experiments, a first-order dependence on cyclobutene **1a**, $PhB(OH)_2$, and the Pd-catalyst was observed. Followed by reductive elimination through the transition state **TS5A-L7-5R6S** (24.9 kcal mol^{-1}), the desired product (1*S*,5*R*,6*S*)-**2a** is produced and active catalyst **INT1A-L7** is regenerated, thus completing the catalytic cycle. The energy barriers for β-hydride elimination *via* the transition states **TS4B-L7-5R6S** and **TS5B-L7-5R6S** are 36.4 and 38.5 kcal mol^{-1}, respectively. Given the reaction temperature of 120 °C, surmounting these energy barriers is extremely challenging. Consequently, the deuterium incorporation associated with the bridging carbon of cyclobutene exhibits remarkable stability (Scheme 3a).

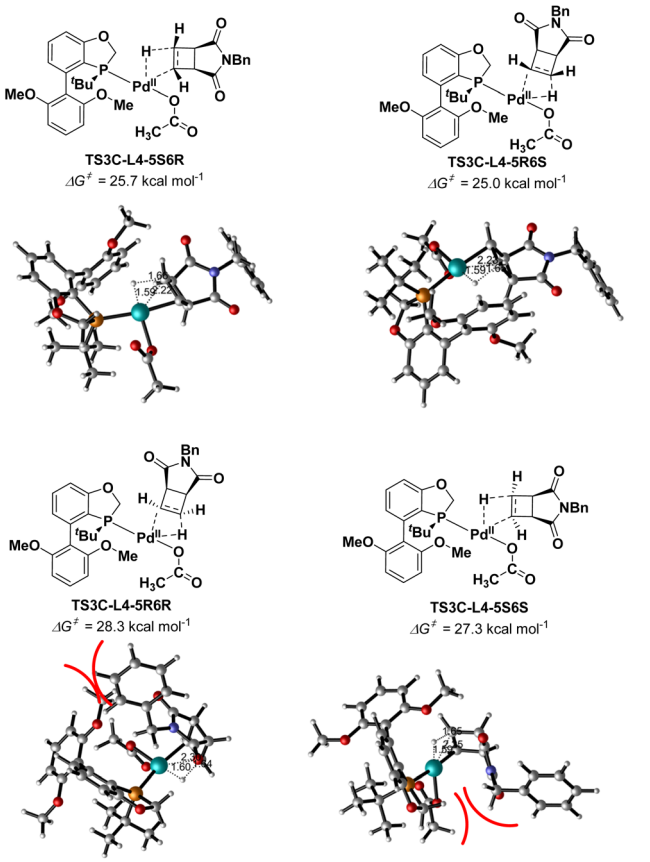

Scheme 5 Competitive pathways for the migratory insertion of **1a** into Pd–H species INT2C-L4.

In comparison to the chiral ligand **L-7** characterized by relatively high rigidity, the utilization of **L-4** as the ligand gives rise to distinct energy profiles that subsequently lead to disparities in deuterium distributions and the formation of products. Specifically, active catalyst **INT1A-L4** is more likely to react with the *in situ* generated acetic acid (HOAc) to form the Pd–H species **INT2C-L4** (Figure S15). By examining the migratory insertion of cyclobutene into Pd–H species **INT2C-L4**, the energies of the transition states **TS3C-L4-5S6R** and **TS3C-L4-5R6S** are determined to be 25.7 kcal mol^{-1} and 25.0 kcal mol^{-1}, respectively (Scheme 5). The calculated difference in the energy barriers between these two transition states amounts to 0.7 kcal mol^{-1}. Such a relatively minor disparity fails to adequately explain the high enantiomeric excess (ee) value observed in the final product **3a**.

A comprehensive investigation was conducted on the subsequent transformation pathways of the generated enantiomers **INT3C-L4-5S6R** and **INT3C-L4-5R6S**. Computational analysis indicates that the enantioselectivity of product **3a** is determined by the selective elimination of β-hydride (Scheme 6). The intermediate **INT3C-L4-5S6R** undergoes β-H elimination through the transition state **TS4C-L4-5S6R**. The calculated energy barrier of this process relative to **INT2C-L4** is 30.0 kcal mol^{-1}. Subsequently, the resulting **INT4C-L4-5S6R** undergoes a second migratory insertion with cyclobutene, leading to the formation of the angular palladium intermediate **INT5C-L4-5S6R**. This step exhibits an energy of 1.4 kcal mol^{-1} lower than that of its enantiomer **INT5C-L4-5R6S** undergoing the same process *via* the transition state **TS5C-L4-5R6S** (31.2 *vs.* 32.6 kcal mol^{-1}). Functioning as the enantio-determining step, it plays a crucial role in determining the predominantly observed 1*R*,5*S*-configuration of product **3a**. Notably, both steps in the transformation from the intermediate **INT3C-L4-5S6R** to **INT5C-L4-5S6R** are reversible, indicating that **INT5C-L4-5S6R** and **INT3C-L4-5S6R** exist in a state of dynamic kinetic equilibrium. Throughout this process, the deuterium atoms in phenylboronic acid can be smoothly incorporated into various positions of the cyclobutane skeleton. This finding is in excellent agreement with the results from deuterium-labeling experiments (Scheme 3e and f). Furthermore, natural population analysis (NPA) shows that the amino group located on the cyclobutyl framework of **INT5A-L4-5S6R** donates supplementary electron density to the metal center (1.174e *vs.* 0.814e).[47] As a result, the electron-rich Pd center can more readily interact with the boron-linked phenyl ring, facilitating β-carbon elimination *via* the transition state **TS6A-L4**. The energy barrier of **TS6A-L4** relative to **INT2A-L4** is 30.7 kcal mol^{-1}, significantly lower than that of the direct β-carbon elimination of **INT3A-L4-5S6R** (30.7 *vs.* 38.3 kcal mol^{-1}, Fig. S19). This difference in energy barriers dictates the regioselectivity of the reaction in the presence of **L-4**. Following the reductive elimination of the intermediate **INT6A-L4**, the desired product (1*S*,5*R*)-**3a** is obtained. The energy barriers for the direct β-carbon elimination processes of the enantiomers **INT3A-L4-5S6R** and **INT3A-L4-5R6S** are 38.3 kcal mol^{-1} and 38.4 kcal mol^{-1} relative to **INT2A-L4**, respectively. Both of these values are higher than the energy barrier of 31.2 kcal mol^{-1} for the β-H elimination process occurring *via* the transition state **TS5C-L4-5S6R**, suggesting that the formation of by-product **2a** is unfavorable kinetically. Given the relatively compact structure of the **L-4** ligand, the steric hindrance between it and the succinimide skeleton is negligible, resulting in an extremely small difference in energy barriers between the two transition states **TS4B-L4-5S6R** and **TS4B-L4-5R6S** (Fig. S19 and S20). Consequently, poor enantioselectivity is observed in the formation of by-product **2a**.

In the absence of $PhB(OH)_2$, the Pd(II)-catalyzed cleavage of the allylic C–H bond proceeds *via* an OAc-assisted concerted metalation-deprotonation (CMD) mechanism (see the SI for details).[66–70] This mechanistic pathway exerts a profound influence on the reaction system, manifesting as a notable reduction in the deuteration incorporation of **1a-D**. This experimental observation dovetails perfectly with the results of the deuterium labeling experiments outlined in Scheme 3d and h, underscoring the coherence and reliability of the proposed reaction mechanism.

The synthetic utility of the 1,3-hydroarylation product was investigated (Scheme 7). Treatment of cyclobutane **3a** with benzylamine afforded amide **4** in 50% yield. Both full and partial reduction of cyclic imide led to the bicyclic products **5** and **6** in good yields. Additionally, allyl-substituted lactam **8** could be prepared *via* a three-step sequence.[75] Furthermore, the reduction of cyclic imide **3a** followed by exposure to acid provided lactone **10** smoothly.

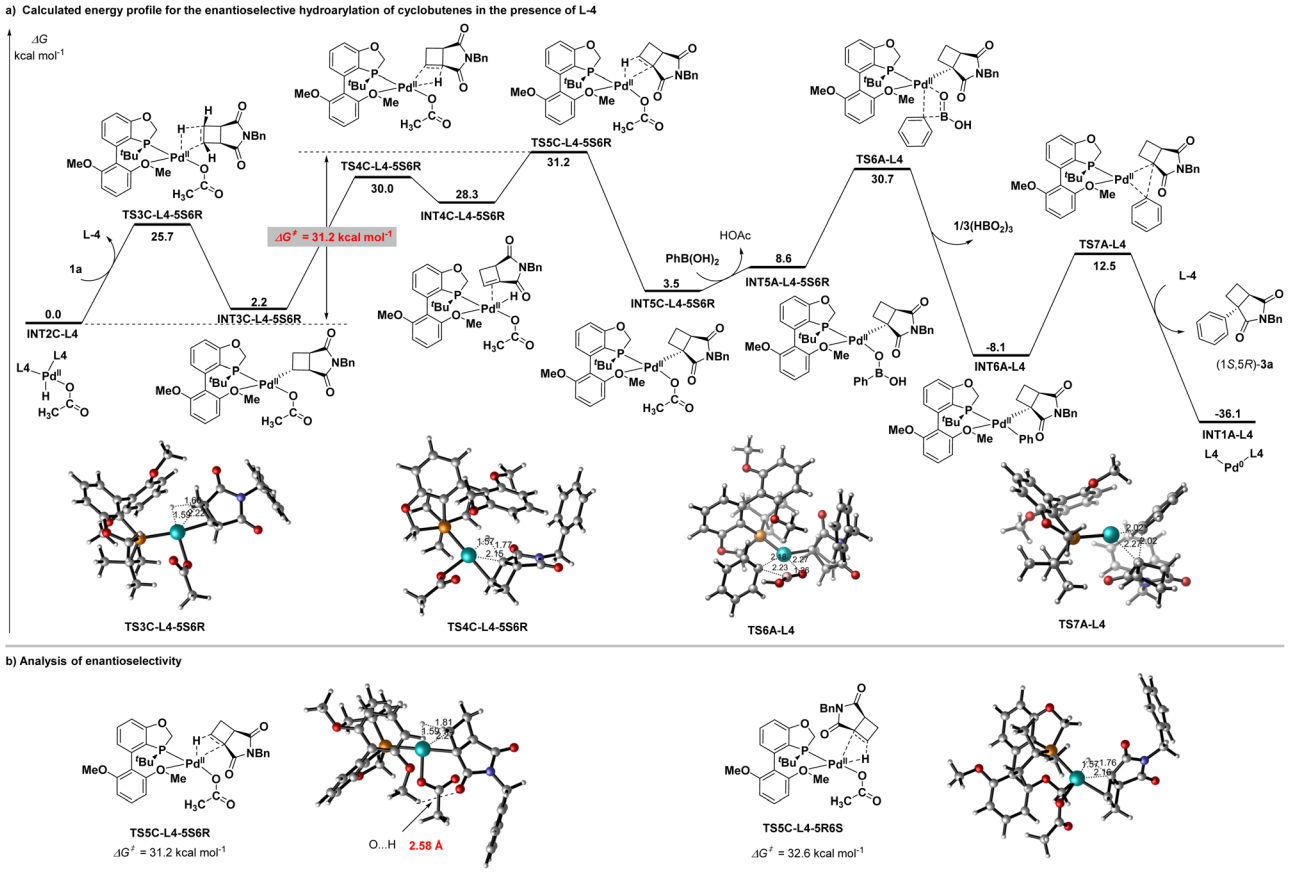

Scheme 6 DFT investigations for the enantioselective 1,3-hydroarylation of cyclobutenes in the presence of L-4.

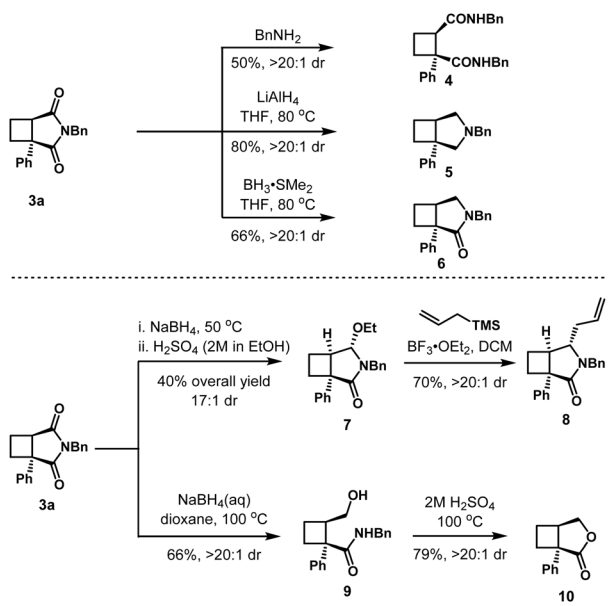

Scheme 7 The further elaboration of hydroarylation product 3a.

Conclusions

We report here a palladium-catalyzed divergent enantioselective functionalization of cyclobutenes with arylboronic acids. With the generation of Pd–H species from palladium with arylboronic acid or *in situ* generated HOAc, two reaction pathways were tuned using two chiral ligands. The reaction process and the origin of enantioselectivity were postulated based on deuterated experiments and DFT calculations. The DFT-calculated mechanistic pathway shows excellent agreement with the deuterium labelling experiments. This agreement not only validates the proposed reaction mechanism but also provides valuable insights into the reaction kinetics and selectivity. We anticipate that these studies could inspire further exploration of unique functionalization methods for strained molecules through transition-metal catalysis.

Author contributions

R. P. and X. Z. conducted the experiments and developed the reactions. J. Z. and M. W. conducted DFT calculations. P. L. conceived the concept. P. L. and M. W. prepared this manuscript.

Conflicts of interest

The authors declare no competing interests.

Data availability

CCDC 2440947 contains the supplementary crystallographic data for this paper.[76]

The data supporting this article have been included as part of the supplementary information (SI). Supplementary information: general information, detailed experimental procedures, characterization data for all new compounds, and NMR spectra. See DOI: https://doi.org/10.1039/d5sc05740j.

Acknowledgements

Financial support from the National Natural Science Foundation of China (grant numbers 22271052 for P. L. and grant number 22171134 for M. W.) and the Natural Science Foundation of Jiangsu Province (Grant BK20240059) is acknowledged. We are also grateful to the High-Performance Computing Center of Nanjing University for performing the numerical calculations in this paper on its blade cluster system.

Notes and references

1 A. de Meijere and F. Diederich, *Metal-Catalyzed Cross-Coupling Reactions*, Wiley-VCH, Weinheim, Germany, 2nd edn, 2004.
2 A. de Meijere, S. Bräse and M. Oestreich, *Metal-Catalyzed Cross-Coupling Reactions and More*, Wiley-VCH, Weinheim, Germany, 2013.
3 D. M. Cartney and P. J. Guiry, *Chem. Soc. Rev.*, 2011, **40**, 5122–5150.
4 R. I. McDonald, G. S. Liu and S. S. Stahl, *Chem. Rev.*, 2011, **111**, 2981–3019.
5 Z. Liu, Y. Gao, T. Zeng and K. M. Engle, *Isr. J. Chem.*, 2020, **60**, 219–229.
6 A. Bahamonde, *Trends Chem.*, 2021, **3**, 863–876.
7 N. Miyaura and A. Suzuki, *Chem. Rev.*, 1995, **95**, 2457–2483.
8 J. Xie, R. Liang and Y. Jia, *Chin. J. Chem.*, 2021, **39**, 710–728.
9 G. Chen, J. Cao, Q. Wang and J. Zhu, *Org. Lett.*, 2020, **22**, 322–325.
10 S. E. Walker, C. J. C. Lamb, N. A. Beattie, P. Nikodemiak and A. L. Lee, *Chem. Commun.*, 2015, **51**, 4089–4092.
11 T.-S. Mei, E. W. Werner, A. J. Burckle and M. S. Sigman, *J. Am. Chem. Soc.*, 2013, **135**, 6830–6833.
12 T.-S. Mei, H. H. Patel and M. S. Sigman, *Nature*, 2014, **508**, 340–344.
13 Q. J. Yuan and M. S. Sigman, *J. Am. Chem. Soc.*, 2018, **140**, 6527–6530.
14 J. B. Liu, Q. J. Yuan, F. D. Toste and M. S. Sigman, *Nat. Chem.*, 2019, **11**, 710–715.
15 Q. J. Yuan, M. B. Prater and M. S. Sigman, *Adv. Synth. Catal.*, 2020, **362**, 326–330.
16 K. Kikushima, J. C. Holder, M. Gatti and B. M. Stoltz, *J. Am. Chem. Soc.*, 2011, **133**, 6902–6905.
17 F. Gini, B. Hessen and A. J. Minnaard, *Org. Lett.*, 2005, **7**, 5309–5312.
18 Q. Xu, R. Zhang, T. Zhang and M. Shi, *J. Org. Chem.*, 2010, **75**, 3935–3937.
19 Y. Iwai, K. M. Gligorich and M. S. Sigman, *Angew. Chem., Int. Ed.*, 2008, **47**, 3219–3222.
20 L. Y. Liao and M. S. Sigman, *J. Am. Chem. Soc.*, 2010, **132**, 10209–10211.
21 S. M. Podhajsky, Y. Iwai, A. Cook-Sneathen and M. S. Sigman, *Tetrahedron*, 2011, **67**, 4435–4441.
22 R. Matsuura, T. C. Jankins, D. E. Hill, K. S. Yang, G. M. Gallego, S. L. Yang, M. Y. He, F. Wang, R. P. Marsters, I. McAlpine and K. M. Engle, *Chem. Sci.*, 2018, **9**, 8363–8368.
23 L.-J. Xiao, L. Cheng, W.-M. Feng, M.-L. Li, J.-H. Xie and Q.-L. Zhou, *Angew. Chem., Int. Ed.*, 2018, **57**, 461–464.
24 H. G. Lv, L. J. Xiao, D. B. Zhao and Q. L. Zhou, *Chem. Sci.*, 2018, **9**, 6839–6843.
25 Y.-G. Chen, B. Shuai, X.-T. Xu, Y.-Q. Li, Q.-L. Yang, H. Qiu, K. Zhang, P. Fang and T.-S. Mei, *J. Am. Chem. Soc.*, 2019, **141**, 3395–3399.
26 X.-Y. Lv, C. Fan, L.-J. Xiao, J.-H. Xie and Q.-L. Zhou, *CCS Chem.*, 2019, **1**, 328–334.
27 J. S. Marcum, T. R. Taylor and S. J. Meek, *Angew. Chem., Int. Ed.*, 2020, **59**, 14070–14075.
28 D. M. Wang, W. Feng, Y. C. Wu, T. Liu and P. Wang, *Angew. Chem., Int. Ed.*, 2020, **59**, 20399–20404.
29 Z. Q. Li, Y. Fu, R. H. Deng, V. T. Tran, Y. Gao, P. Liu and K. M. Engle, *Angew. Chem., Int. Ed.*, 2020, **59**, 23306–23312.
30 Y. He, C. Liu, L. Yu and S. Zhu, *Angew. Chem., Int. Ed.*, 2020, **59**, 9186–9191.
31 K. Chen, H. Zhu, S. Liu, J. Bai, Y. Guo, K. Ding, Q. Peng and X. Wang, *J. Am. Chem. Soc.*, 2023, **145**, 24877–24888.
32 H.-D. He, R. Chitrakar, Z.-W. Cao, D.-M. Wang, L.-Q. She, P.-G. Zhao, Y. Wu, Y.-Q. Xu, Z.-Y. Cao and P. Wang, *Angew. Chem., Int. Ed.*, 2024, **63**, e202313336.
33 M. Wang and P. Lu, *Org. Chem. Front.*, 2018, **5**, 254–259.
34 M. R. Bauer, P. D. Fruscia, S. C. C. Lucas, L. N. Michaelides, J. E. Nelson, R. L. Storer and B. C. Whitehurst, *RSC Med. Chem.*, 2021, **12**, 448–471.
35 J. Chen, Q. Zhou, H. Y. Fang and P. Lu, *Chin. J. Chem.*, 2022, **40**, 1346–1358.
36 L. Nóvoa, L. Trulli, A. Parra and M. Tortosa, *Angew. Chem., Int. Ed.*, 2021, **60**, 11763–11768.
37 D. J. Konowalchuk and D. G. Hall, *Angew. Chem., Int. Ed.*, 2023, **62**, e202313503.
38 M. Yan, Q. Zhou and P. Lu, *Angew. Chem., Int. Ed.*, 2023, **62**, e202218008.
39 D. Egea-Arrebola, F. W. Goetzke and S. P. Fletcher, *Angew. Chem., Int. Ed.*, 2023, **62**, e202217381.
40 Z. K. Liang, L. Wang, Y. Wang, L. F. Wang, Q. L. Chong and F. K. Meng, *J. Am. Chem. Soc.*, 2023, **145**, 3588–3598.
41 S. Lan, H. J. Huang, W. J. Liu, C. Xu, X. Lei, W. Dong, J. G. Liu, S. Yang, A. E. Cotman, Q. Zhang and X. Q. Fang, *J. Am. Chem. Soc.*, 2024, **146**, 4942–4957.
42 F. S. Yuan, X. Y. Qi, Y. Y. Zhao, J. Jia, X. F. Yan, F. D. Hu and Y. Xia, *Angew. Chem., Int. Ed.*, 2024, **63**, e202401451.
43 Q. Wu, Z. Zhang, Q. Chong and F. Meng, *Angew. Chem., Int. Ed.*, 2025, **64**, e20241652.
44 R. Pan and P. Lu, *Chin. J. Chem.*, 2025, **43**, 184–190.
45 N. J. McAlpine, L. Wang and B. P. Carrow, *J. Am. Chem. Soc.*, 2018, **140**, 13634–13639.
46 F. W. Goetzke, A. M. L. Hell, L. van Dijk and S. P. Fletcher, *Nat. Chem.*, 2021, **13**, 880–886.

47 Z. Wang, J. Zhu, M. Wang and P. Lu, *J. Am. Chem. Soc.*, 2024, **146**, 12691–12701.
48 J. Corpas, P. Mauleón, R. G. Arrayás and J. C. Carretero, *ACS Catal.*, 2021, **11**, 7513–7551.
49 N. J. Adamson and S. J. Malcolmson, *ACS Catal.*, 2020, **10**, 1060–1076.
50 B. M. Trost, *Chem. – Eur. J.*, 1998, **4**, 2405–2412.
51 G. Li, X. Huo, X. Jiang and W. Zhang, *Chem. Soc. Rev.*, 2020, **49**, 2060–2118.
52 A. Y. Jiu, H. S. Slocumb, C. S. Yeung, X.-H. Yang and V. M. Dong, *Angew. Chem., Int. Ed.*, 2021, **60**, 19660–19664.
53 S.-Z. Nie, R. T. Davison and V. M. Dong, *J. Am. Chem. Soc.*, 2018, **140**, 16450–16454.
54 Z. Liu, J. Derosa and K. M. Engle, *J. Am. Chem. Soc.*, 2016, **138**, 13076–13081.
55 O. Löber, M. Kawatsura and J. F. Hartwig, *J. Am. Chem. Soc.*, 2001, **123**, 4366–4367.
56 S.-Q. Yang, A.-J. Han, Y. Liu, X.-Y. Tang, G.-Q. Lin and Z.-T. He, *J. Am. Chem. Soc.*, 2023, **145**, 3915–3925.
57 N. J. Adamson, E. Hull and S. J. Malcolmson, *J. Am. Chem. Soc.*, 2017, **139**, 7180–7183.
58 C. H. Oh, H. H. Jung, K. S. Kim and N. Kim, *Angew. Chem., Int. Ed.*, 2005, **42**, 805–808.
59 M.-M. Li, L. Cheng, L.-J. Xiao, J.-H. Xie and Q.-L. Zhou, *Angew. Chem., Int. Ed.*, 2021, **60**, 2948–2951.
60 Q. Zhang, D. Dong and W. Zi, *J. Am. Chem. Soc.*, 2020, **142**, 15860–15869.
61 J. Corpas, P. Mauleón, R. G. Arrayás and J. C. Carretero, *Org. Lett.*, 2020, **22**, 6473–6478.
62 N. J. Adamson, K. C. E. Wilbur and S. J. Malcolmson, *J. Am. Chem. Soc.*, 2018, **140**, 2761–2764.
63 S. Friedman, B. Pace and R. Pizer, *J. Am. Chem. Soc.*, 1974, **96**, 5381–5384.
64 T. Yasukawa, H. Nakajima, R. Masuda, Y. Yamashita and S. Kobayashi, *J. Org. Chem.*, 2022, **87**, 13750–13756.
65 Á. Magyar, K. Juhász and Z. Hell, *Synthesis*, 2021, **53**, 279–295.
66 D. L. Davies, S. A. Macgregor and C. L. McMullin, *Chem. Rev.*, 2017, **117**, 8649–8709.
67 D. García-Cuadrado, A. A. C. Braga, F. Maseras and A. M. Echavarren, *J. Am. Chem. Soc.*, 2006, **128**, 1066–1067.
68 S. I. Gorelsky, D. Lapointe and K. Fagnou, *J. Am. Chem. Soc.*, 2008, **130**, 10848–10849.
69 D. Lapointe and K. Fagnou, *Chem. Lett.*, 2010, **39**, 1118–1126.
70 L. Wang and B. P. Carrow, *ACS Catal.*, 2019, **9**, 6821–6836.
71 All calculations were performed at the B3LYP-D3BJ/6-311+G(d,p)-SDD(Pd)/IEFPCM(benzene or toluene)//B3LYP-D3BJ/6-31G(d)-SDD(Pd) level of theory using Gaussian 09 software package (see SI for details).
72 L. P. E. Yunker, Z. Ahmadi, J. R. Logan, W. Wu, T. Li, A. Martindale, A. G. Oliver and J. S. McIndoe, *Organometallics*, 2018, **37**, 4297–4308.
73 K. Osakada and Y. Nishihara, *Dalton Trans.*, 2022, **51**, 777–796.
74 A. A. Thomas and S. E. Denmark, *Science*, 2016, **352**, 329–332.
75 M. Ostendorf, R. Romagnoli, I. C. Pereiro, E. C. Roos, M. J. Moolenaar, W. N. Speckamp and H. Hiemstra, *Tetrahedron: Asymmetry*, 1997, **8**, 1773–1789.
76 CCDC 2440947: Experimental Crystal Structure Determination, 2025, DOI: **10.5517/ccdc.csd.cc2my07v**.